REPORT NUMBER (18) (19) AFOSR-TR-78-1013	2. GOVT ACCESSION NO.
3. RECIPIENT'S CATALOG NUMBER	
4. TITLE (and Subtitle) Calibration and Evaluation of the Long Period (> 100 sec) Properties of the Geotech Model 36000 Borehole Seismometer System, (6)	5. TYPE OF REPORT & PERIOD COVERED Final Technical 7/02/76-12/31/77 (2)
	6. PERFORMING ORG. REPORT NUMBER
7. AUTHOR(s) (10) Jonathan Berger and Freeman Gilbert	8. CONTRACT OR GRANT NUMBER(s) (15) F49620-76-C-0032 ARPA Order-3291
9. PERFORMING ORGANIZATION NAME AND ADDRESS The Regents of the University of California San Diego, California 92093	10. PROGRAM ELEMENT, PROJECT, TASK AREA & WORK UNIT NUMBERS A.O. 3291, PC TF-10 Element 62701E
11. CONTROLLING OFFICE NAME AND ADDRESS ARPA/NMR 1400 Wilson Boulevard Arlington, VA 22209 (11) 14 Aug 78	12. REPORT DATE 04/07/78 Revised 8/14/78
	13. NUMBER OF PAGES 45
14. MONITORING AGENCY NAME & ADDRESS (if different from Controlling Office) AFOSR/NP Bolling AFB, Bldg. 410 Washington, DC 20332 (12) 59 p.	15. SECURITY CLASS. (of this report) Unclassified
	15a. DECLASSIFICATION/DOWNGRADING SCHEDULE

16. DISTRIBUTION STATEMENT (of this Report)

Approved for public release, distribution unlimited

(9) Final technical rept. 2 Jul 76-31 Dec 77

LEVEL II

DDC

17. DISTRIBUTION STATEMENT (of the abstract entered in Block 20, if different from Report)

RECEIVED SEP 14 1978 A

18. SUPPLEMENTARY NOTES

PLEASE NOTE: This is a revised Final Technical Report.
Supersedes AD54788

19. KEY WORDS (Continue on reverse side if necessary and identify by block number)

20. ABSTRACT (Continue on reverse side if necessary and identify by block number)

The parametric modelling of the Geotech Model 36000 seismic system is described. A compact representation for the linear part of the system transfer function is developed and a rapid and accurate method of determining the parametric coefficients is demonstrated.

DD FORM 1 JAN 73 1473 EDITION OF 1 NOV 65 IS OBSOLETE

SECURITY CLASSIFICATION OF THIS PAGE (When Data Entered)

012 380

AFOSR-TR-78-1013

FINAL TECHNICAL REPORT

REVISED 8/14/78

Principal Investigators

Jonathan Berger and Freeman Gilbert

Sponsored by
Advanced Research Projects Agency (DOD)
ARPA Order No. 3291
Monitored by AFOSR Under Contract # F49620-76-C-0032

1. INTRODUCTION

A Geotech Model KS 36000-01 seismic system was obtained on loan from the USGS in Albuquerque and operated in our La Jolla labs for several months during 1977. We endeavored to study the system's response characteristics over its operating band and develop methods of modeling that response. We have developed a rapid and very accurate method of linear calibration which results in a compact representation of the system response.

Due to the extremely high ambient noise in the La Jolla site, we were not able to investigate system nonlinearities and had planned to carry out that part of the research project with the instrument installed in a bore hole at Piñon Flat Observatory, however, this part of the research was not funded.

We began by developing a parametric linear system model using the instrument description provided by the manufacturer's manuals. We then tested these models to discover if they accurately described the system which we had installed.

In the linear approximation, we show that the system models yield an input-output equation (in Laplace transform domain)

$$E_{out}(s) = T_p(s) \left\{ A_g(s) - G_4 \quad E_c(s) \right\} \tag{1.1}$$

where $A_g(s)$ is ground acceleration, G_4 is the forcing constant acting on calibration voltage $E_c(s)$ and $T_p(s)$ (p for parameterized) is the system transfer function. Furthermore, $T_p(s)$ is itself the ratio of two polynomials in s with real coefficients that depend on known instrument parameters

$$T_p(s) = \frac{N(s)}{D(s)} \quad . \tag{1.2}$$

We describe how the coefficients of polynomials N and D in Eq. 1.2 are more or less accurately found, but conclude that this is not a good calibration method. We have found that better results can more easily be obtained by inserting pseudo random signals for E_c, estimating $T(i\omega)$ by cross-spectral analysis and finally deriving $T(s)$ by analytic continuation into the complex s-plane.

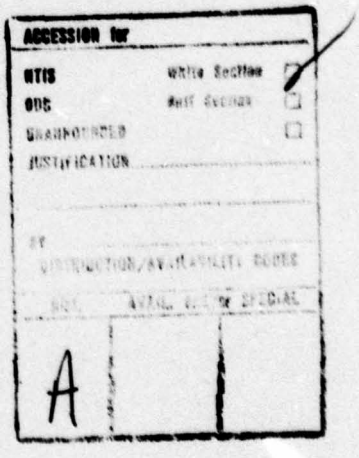

2. THE PARAMETRIC MODEL

The SRO instrument is a 3-axis seismograph system (the Geotech Model KS 36000-01), designed for installation in a borehole. We present here an abbreviated discussion of the vertically oriented accelerometer, but the behavior of the horizontal sensors is not significantly different. The SRO system manuals (Teledyne-Geotech, 1975) give a more complete discussion. (See also McCowan and Lacoss, 1978.)

The vertical accelerometer is built around a La Coste-type pendulum with a highly underdamped 5 to 10 sec period. The position of the mass is sensed by a capacitive transducer and the feedback force is applied electromagnetically through a coil magnet arrangement. Electronic feedback is used to alter the system characteristics so that the response matches that of a 1 Hz pendulum damped 0.8 of critical.

There is no provision for mechanically adjusting the equilibrium position of the mass and therefore the dynamic range of the electrical force must be sufficient to null the gravitational force at any latitude. From the pole to the equator, g changes by about 5×10^{-2} ms^{-2} . Thus, with a 20V dynamic range available, the closed loop response at dc cannot exceed 400 volts m^{-1} s^2 without restricting where the instrument can operate. This low loop gain makes it difficult to resolve ground noise at the low end of the normal mode band 10^{-3} Hz to 10^{-2} Hz as the equivalent voltages on the loop are about 3×10^{-10} V rms over this band (Agnew and Berger, 1978). For shorter periods, the loop signal is high passed with a corner at 50 sec and amplified by 2000 before it is sent "up-hole." Thus at the surface, the basic data channel has a sensitivity of 10^6 V m^{-1} s^2 from 50 sec to 1 sec.

The SRO circuits are described elsewhere (Geotech, 1975), so we give just an abbreviated development of the loop response starting with the block diagram of Figure 1.

The response of the pendulum to an external acceleration is

$$\ddot{e}_1 + 2\zeta\Omega\dot{e}_1 + \Omega^2 e_1 = a_g - a_f \qquad (2.1)$$

where e_1 is the displacement of the mass, ζ the damping and Ω the radian frequency of oscillation. The transfer function of the transducer is

$$T_1(s) = \frac{1}{s^2 + 2\zeta\Omega s + \Omega^2} \quad .$$

The displacement transducer, modulator and amplifier have a total transfer function, G_2, which is frequency independent over the range of interest.

The next three blocks in the loop block diagram (see Figure 2, upper panel) must be examined in total to obtain their overall transfer function. Referring to Figure 2

$$(e_2 + e_i)A = e_{out} \text{ and } e_2 = -e_1$$

so

$$(e_i - e_1)A = e_{out} \quad . \qquad (2.2)$$

Taking Laplace transforms

$$E_1 = \frac{E_D + E_{out}\, s\tau_1}{1 + s\tau_1} \qquad (2.3)$$

where $\tau_1 = R_1 C_1$. However, $E_D = -A\, E_1$ and so

$$E_1 = \frac{s\tau_1}{(1 + A) + s\tau_1}\, E_{out} \quad . \qquad (2.4)$$

Using the Laplace transform of (2.2) to eliminate E_1

$$\frac{E_{out}}{E_i} = A\left[\frac{1 + A + s\tau_1}{(1 + A)(1 + s\tau_1)}\right] \quad . \tag{2.5}$$

The demodulator amplifier, here represented by A, consists of a single pole low pass filter with transfer function

$$A = \frac{G_5 p_D}{s + p_D} \tag{2.6}$$

and gain G_5 is 200, with $p_D = 100\ s^{-1}$. We then write (2.5) as

$$\frac{E_{out}}{E_i} = \frac{G_5 p_D}{s + p_D}\left[\frac{s^2 + sp_D + z_2 p_D}{(s+G_5 p_D)(s+p_2)}\right] \tag{2.7}$$

where $z_2 = G_5/\tau_1$, $p_2 = 1/\tau_1$ and the approximation $G_5 >> 1$ is used. The numerator of (2.7) can be approximately factored as

$$(s^2 + p_D s + z_2 p_D) \approx (s + z_2)(s + p_D) \quad \text{since } p_D >> z_2 ,$$

so finally we have to good accuracy

$$\frac{E_{out}}{E_i} = \frac{G_5\ p_D}{s + G_5 p_D}\left[\frac{s + z_2}{s + p_2}\right] \quad .$$

The part outside the brackets is the response of low pass filter with reciprocal time constant $G_5 p_D \approx 2 \times 10^4$ and hence may be ignored.

Thus we write the transfer function T_2 as

$$T_2(s) = G_2\left[\frac{s + z_2}{s + p_2}\right] \quad . \tag{2.8}$$

The remaining elements in the feedback loop are shown in the lower panel of Figure 2 . At frequencies of interest, the resistive impedance of the forcing coil is much greater than the inductive impedance. Further, the resistive impedance is much smaller than either the impedance of the compensator or R_{cal} . With these approximations

$$T_3(s) = G_3 R_c \left(\frac{s + z_3}{s + p_3}\right)$$

where

$$G_3 = \frac{p_3}{R_2 z_3} \quad , \quad p_3 = \frac{1}{R_3 C_2} \quad , \quad \text{and} \quad z_3 = \frac{1}{(R_2 + R_3)\, C_2}$$

and $$T_{cal} = \frac{R_c}{R_{cal}} \quad .$$

The forcing coil constant is G_4 (ms^{-2}/amp) so that T_4 is given by

$$T_4 = \frac{G_4}{R_c} \quad .$$

We may now draw the simplified signal flow graph shown in Figure 3 . The closed loop transfer function obtained from this is

$$T(s) = \frac{T_1(s)\, T_2(s)}{1 + T_1(s)\, T_2(s)\, T_3(s)\, T_4(s)}$$

$$= \frac{G_2(s + z_2)\,(s + p_3)}{(s^2 + 2\zeta\Omega s + \Omega^2)(s + p_2)\,(s + p_3) + G_2 G_3 G_4 (s + z_2)\,(s + z_3)} \quad . \qquad (2.9)$$

At low frequencies, the loop response tends to the constant

$$\lim_{s\to o} T(s) = \frac{G_2 z_2 p_3}{\Omega^2 p_2 p_3 + G_2 G_3 G_4 z_2 z_3} .$$

With the suite of instrumental parameters given in Table 1 , it is clear that

$$\lim_{s\to o} T(s) = \frac{p_3}{G_3 G_4 z_3} = \frac{R_2}{G_4} = 516 \text{ V m}^{-1} \text{ s}^2 \qquad (2.10)$$

The data output E_D is related to the system output E_{out} by (2.4);

$$E_D = - A \frac{s\tau_1}{(1 + A) + s\tau_1} E_{out}$$

Using (2.6) and substituting p_5 for G_5/τ_1 we obtain

$$\frac{E_D}{E_{out}} = - \frac{G_5 p_D s}{s^2 + p_D s + p_D p_5 + p_2}$$

where we have made the approximation $G_5 >> 1$. This can be factored approximately by noting that $p_D >> p_5 , p_2$ to yield

$$T_5(s) = \frac{G_5 p_D s}{(s + p_D)(s + p_5)} . \qquad (2.11)$$

This describes a band pass filter with a gain of 200 between 50 sec and 16 Hz.

The response of the system may be analyzed with the help of a root locus plot, Figure 4 , of the transfer function, Eq. (2.9). The poles of the system are the solutions of

$$(s^2 + 2\zeta\Omega s + \Omega^2)(s + p_2)(s + p_3) + G(s + z_2)(s + z_3) = 0 \qquad (2.12)$$

where $G = G_2G_3G_4$ and the root locus follows these roots as the open loop gain G is varied. The locii of the roots move from the solutions for $G = 0$ to the roots when $G \to \infty$. The open loop poles ($G = 0$) are at

$$s = -p_3 = -50 \; ; \; s = -p_2 = -6.25 \times 10^{-4}$$

and a complex conjugate pair corresponding to the unfedback pendulum of

$$s = -2.21 \times 10^{-2} \pm 1.25 \, i \; .$$

Table 1 gives the values of parameters for the particular Model 36000 system we analyzed. With the exception of G_2, all parameter values given in this table were taken from the Geotech manual. If we take $\Omega = 1.25$ and $\zeta = .0177$ and use the G_2 given in the manual (1.968×10^4 V m^{-1}) we find a polynomial for $T_p(s)$ close to that of McCowan and Lacoss (1978) with the exceptions pointed out by Berger *et al.* (1978). This implies an operating point marked by Θ on the root locus of Figure 4.

However, we calibrated a Model 36000 and found that the polynomial which best fit the measured response was significantly different with an implied operating point near A in Figure 4. A careful study of the operating manuals led us to the conclusion that all parameters except G_2 are accurately controlled or measured for each individual unit. We, therefore, made our own estimate of G_2 as follows.

The roots of the denominator of the transfer function polynomial (2.12) are approximately solutions of

$$s^4 + p_3 \, s^3 + (p_3\Omega^2 + GZ_3) \, s + GZ_2Z_3 = 0$$

where $G = G_2G_3G_4$. Taking the parameter values from Table 1 with $\Omega = 1.25$

and leaving G_2 as a variable we solve for the value of G_2 which gives a pair of complex roots closest in the rms vector sense to the corresponding pair we recovered experimentally, letting the other two roots lie where they may. The process leads to our estimate of $G_2 = 1{,}31 \times 10^4$ V m^{-1} ± 5 percent. Using this value, we have the overall transfer function for the mass position output of

$$T_{pM}(s) = \left[\frac{2.59 \times 10^4}{s^2 + 8.50\ s + 32.6}\right] \left\{\frac{(s + 50)\ (s + .125)}{(s + 41.4)\ (s + .118)}\right\} \text{ V m}^{-1}\ \text{s}^2 \qquad (2.13)$$

where a factor of 2 is included to account for the down hole line driver on this signal.

The corresponding expression for the data output channels is obtained by multiplying (2.13) by T_5 (2.9) to yield

$$T_{pD}(s) = \left[\frac{2.59 \times 10^9}{s^2 + 8.50\ s + 32.6}\right] \left\{\frac{s(s + 50)}{(s + 41.4)\ (s + .118)\ (s + 100)}\right\} \text{V m}^{-1}\ \text{s}^2 \qquad (2.14)$$

where we have included the gain of 10 in the data output line drivers.

As noted by Berger *et al.* (1978) the differences in response between these expressions and those of McCowan and Lacoss (1978) are significant for frequencies above 1 Hz.

Figure 5 shows the sensitivity of the position of one of the dominant poles as certain system parameters are varied. Figure 6 shows the Bode plots of the two system outputs.

Table 1.

Nominal SRO instrumental parameters

Ω = .628 to 1.25	G_2 = 1.31 x 10^4 V m^{-1}
ζ ≤ .0177	G_3 = 2.14 x 10^{-3} ohm^{-1}
R_c = 25 ohm	G_4 = 13.95 ms^{-2} amp^{-1}
R_2 = 7204 ohm	G_5 = 200
τ_1 = 1.6 x 10^3	P_2 = 6.25 x 10^{-4}
R_3 = 500 ohm	P_3 = 50
C_2 = 40 μfd	P_5 = .125
	P_D = 100
	z_2 = .125
	z_3 = 3.24

3. THE CROSS-SPECTRAL CALIBRATION TECHNIQUE

The essence of this technique to determine the system's frequency response (or transfer function) is the calculation of the cross-spectrum between a known calibrating signal and the system output. The use of cross-spectral methods minimizes the effects of noise which are unavoidably present in the form of ground noise or internally generated electronic noise. The transfer function calculated from the cross-spectrum, though adequate, is not the most convenient way to express the frequency response of the system. The results of the parametric modeling suggest a more compact representation, namely the ratio of two complex polynomials (or equivalently, their roots). We have developed a method for finding these polynomials from the cross-spectral estimates.

In the following sections we deal with the type of input function to be used, the cross-spectral methods, and the techniques for finding the system polynomial. Finally, we illustrate the method on the system installed in our labs.

3.1 The Calibrating Signal

To measure the frequency response across the instrumental passband requires that the calibrating signal be more powerful than the noise (ground and instrumental) throughout that band. The most common choices for input signals are impulses and steps. Impulses are broad band, but must be applied at low level to ensure the peak signal does not exceed the dynamic range of the system. Steps may be input at much higher levels, but the spectral power density of a step

falls off as ω^{-2} so that much of the power is confined to low frequencies. Because we use cross-spectral methods, there is no premium on using simple signals. The calibrating signal we use is a pseudo-random binary signal (RB), which can be input at the high level used for a step, but has power distributed over a broad band of frequencies.

The RB signal (MacWilliams and Sloan, 1976), and its relative the random telegraph (RT) signal (Jenkins and Watts, 1968 p. 170) are well known to electrical engineers and have seen seismological application by Moore and Farrell (1970), among others. There is a vast literature so we give just the salient properties.

The RB and RT signals can be viewed as sequences of step functions of fixed amplitude but alternating polarity. The duration of each step is a random function of time. The probability density function for the step durations of the RT signal is uniformly distributed over continuous time, but for the RB singal the length of each step is a (random) integral multiple of some basic time interval τ . Stated differently, the RB signal is a binary signal which has a 50% chance of changing state at discrete times $n\tau$ $(n = 1, 2 \ldots)$.

Random binary signals are easily generated by periodically clocking a long shift register at fixed interval τ . For a shift register of specified length, a particular feedback arrangement exists (Lancaster, 1975) which assures that the output for all practical purposes is equivalent to a RB signal. (A feedback shift register of n stages has at most $n - 1$ distinct states, so the output is actually periodic, but a modest number of stages ensures that the period will be orders of magnitude longer than the duration of our experiments.)

The power spectrum of a section of RB signal of amplitude V volts peak to peak and clocked at interval τ is approximately

$$P(\omega) = \frac{V^2\tau}{4} \left(\frac{\sin \omega\tau/2}{\omega\tau/2}\right)^2 \quad \text{volts}^2/\text{Hz} \qquad (3.1)$$

In Equation (3.1) we neglect the spectral discreteness caused by the shift register periodicity. It is unimportant compared with the discreteness caused by the truncation of the sequence which always occurs in practice, and we assume that the spectrum of any sample extracted from the sequence is the same as the spectrum of the entire sequence. The important point is that the spectrum is quite flat up to the -3 db frequency $\omega = 2/\tau$.

Even though the RB sequence is a broad band signal, its special form allows it to be more infrequently sampled than the Nyquist theorem. As the shortest possible pause in either state is the clock period τ, samples taken at interval τ allow exact reconstruction of the entire waveform. This reconstruction is vastly simplified if the sample times are synchronized to the shift register clock as is our practice.

3.2 Calibration Using Random-Binary Signals

The symmetric voltage generated by the RB generator is added to the system feedback loop. The RB period is set so that the first "hole" in the RB spectrum occurs at a frequency higher than that of the dominant poles of the system (see Section 2). The RB amplitude is set to the highest level possible without instrument (or data filter) saturation.

The RB generator is synchronized with the data recorder clock to avoid aliasing problems and assist in the reconstruction of the signal form. Both the RB input and the systems output are recorded at an appropriate sample interval for a total period of something like 10 times the longest period of interest.

4. CROSS-SPECTRUM ESTIMATION OF THE TRANSFER FUNCTION

Using a RB signal to perturb the closed loop accelerometer, we calculate an estimate, $\hat{T}(i\omega)$, of the transfer function $T(s)$ evaluated along the real (radian) frequency axis $s = i\omega$ by calculating the cross spectrum between e_c, the calibration signal, and e_{out} the system output signal. In the noise free case the transfer function can be found simply by dividing the output spectrum by the input spectrum, but when there is noise, such a procedure leads to bias (Munk and Cartwright, 1966). This bias may be reduced by dividing the cross-spectrum by the input spectrum to determine the transfer function. However, sample cross-spectral estimates are themselves biased if there are large delays between the input and output series (Jenkins and Watts, 1968, Ch. 9), so that we must use a more complicated procedure. What we do is to modify the input function in a known way so as to make it look like the output. The delays between the two signals (and hence the phase of the cross-spectrum) will then be small, and the bias in the cross-spectrum greatly reduced. Jenkins and Watts (1968, Ch. 9) discuss one way to do this, which is to shift one series relative to the other, a technique they term alignment. This simple device has proved insufficient for our needs, and we have used a more elaborate technique, which we call prefiltering.

We convolve the record of the calibrating voltage (e_c, Figure 7) with an approximation of the system impulse response. (Because of the form of our input, we actually use a first-differenced step response rather than an impulse response; this is discussed in Section 2.) The predicted output so produced (e'_{out}) closely resembles the actual recorded output. Since the system acts essentially as a low pass filter, e'_{out} has much

less bandwidth than the RB signal so that aliasing is unimportant. We then form the cross-spectrum between the predicted output (e'_{out}) and recorded output (e_{out}), and use it to correct our approximate response. This corrected response gives us our estimate of the transfer function.

Recalling Equation (1.1)

$$E_{out} = T\left(A_g - G_4 E_c\right) \tag{4.1}$$

where T is the transfer function we are to calculate, A_g and E_c the Fourier transforms of the ground acceleration and RB voltage signal respectively, and G_4 the feedback constant. The Fourier transform of the predicted output is

$$E'_{out} = -G_4 T_0 E_c \tag{4.2}$$

where T_0 is our first guess of T.

Let C_{11} be the spectrum of E'_{out}, C_{22} the spectrum of E_{out} and C_{12} the cross-spectrum. Then

$$C_{11} = |G_4 T_0|^2 E_c^* E_c \tag{4.3}$$

$$C_{22} = E_{out}^* E_{out} \tag{4.4}$$

$$C_{12} = -G_4 T_0^* E_c^* E_{out} \tag{4.5}$$

where, in the equations, the frequency dependence of the functions has been suppressed, the asterisks denote complex conjugation and $||$ denote the magnitude of the enclosed quantity.

Using Equation (4.1) we rewrite Equation (4.5)

$$C_{12} = G_4 T_0^* \; T(-E_c^* A_g + G_4 E_c^* E_c) \; . \tag{4.6}$$

The cross-spectrum, C_{12}, contains an unwanted contribution from earth noise, A_g, but because e_c and a_g are uncorrelated, estimates of the cross power term $E_c^* A_g$, separated in frequency by the reciprocal record length or more, are statistically independent. Thus, the earth noise term in Equation (4.6) can be reduced by smoothing in the frequency domain.

The method of segment averaging is used to obtain smoothed spectral estimates (Bendat and Piersol, 1971, p.328; Haubrich, 1965). In this method the original series is divided into M sections. Each section is tapered and Fourier transformed to yield M estimates of the powers C_{ij}. The individual estimates at each frequency are averaged, yielding smoothed spectral estimates with approximately 2M degrees of freedom.

Using an overbar to denote the smoothed spectra, we get

$$\overline{C_{11}} = \overline{|G_5 T_0|^2} \quad \overline{|E_c|^2} \tag{4.7}$$

$$\overline{C_{22}} = \overline{|T|^2} \left(\overline{|A_g|^2} + G_5^2 \, \overline{|E_c|^2} \right) \tag{4.8}$$

$$\overline{C_{12}} = G_5 \quad \overline{|T_0^* T|} \quad \overline{|E_c|^2} \tag{4.9}$$

We have assumed here that perfect averaging has made $\overline{E_c^* A_g} = 0$ in going from (4.6) to (4.9), which is never true for a finite amount of data, a point we return to later.

Let T_Δ be the ratio of the cross spectrum to the (modified) input spectrum

$$T_\Delta = \overline{C_{12}} \Big/ \overline{C_{11}} = \overline{T_0^* T} \Big/ \overline{T_0^* T_0} \quad . \tag{4.10}$$

Then we take as the estimate of the transfer function

$$\hat{T} = T_0 T_\Delta \tag{4.11}$$

where we have assumed that T_0 is so close to T that the ratio of the averaged spectra is the same as the average of the ratio.

If T_Δ differs significantly from 1, then $\hat{T}$ can be used as a next approximation to T and the procedure repeated, but we have never had to use this iterative refinement.

4.1 Confidence Limits on the Transfer Function Estimates

The estimated and true transfer functions will in general be different because of the noise in the measured signal. The random variable

$$r^2 = |\hat{T} - T|^2 \tag{4.12}$$

(which is a measure of this difference) follows an $F_{2,\nu-2}$ distribution (see Jenkins and Watts, 1968, pp.85-87) where ν is the $2M$, the number of segments into which the series is divided for analysis. Jenkins and Watts (1968, Sec. 10.3) further show that

$$\frac{r_{95}}{|\hat{T}|} = \left[\frac{2}{\nu-2} F_{2,\nu-2}(.05)\right]^{\frac{1}{2}} \left[\frac{1-\hat{\gamma}_{12}^2}{\hat{\gamma}_{12}^2}\right]^{\frac{1}{2}} \tag{4.13}$$

where r_{95} is the expected value of r at a 95 percent confidence level, and $\hat{\gamma}_{12}$ is the estimated coherence between E_{out} and E'_{out}.

Obviously we desire r_{95} to be as small as possible. Figure 8 shows how the expected error varies with the number of data segments and the coherence. We see that to obtain an error of 1 percent with a reasonable number of data segments a very high coherence ($\hat{\gamma}^2_{12} > .999$) is required. Fortunately it is not hard to achieve such high levels of coherence, because the great dynamic range of most instruments permits the use of a strong RB calibration signal (50 db above earth noise) without danger of saturating the system. It is worth observing here that without prefiltering estimated coherences are biased downward, making the error estimate unnecessarily pessimistic; prefiltering substantially eliminates phase shift between the output signal and input thereby allowing the estimated coherence to attain its true value (see Figure 9).

We generally work with $\nu \geq 50$ and under these conditions of large ν the $F_{2,\nu-2}$ distribution closely approximates X^2 with two degrees of freedom. This suggests that our conditions now approach those analyzed by Munk and Cartwright (1966, Appendix B) who showed that error in the real and imaginary parts of the transfer function are independent, and normally distributed with the same variance. This assumption is extremely useful in fitting the transfer function with a rational approximation as we shall see in the next section.

5. RATIONAL FUNCTION APPROXIMATION TO THE TRANSFER FUNCTION

The linear analysis of the seismometer in Sec. 2 leads us to the representation of T in terms of a ratio of two polynomials in s, or equivalently $i\omega$. Having estimated the transfer function $\hat{T}$ at frequencies ω_k, $k = 1, 2 \ldots m$, along the imaginary S-plane axis as described in the previous section, we can now obtain estimates of the coefficients of the polynomials by fitting $\hat{T}$ to the model given by the linear theory. As a function of frequency the complex response must be of the form:

$$T(i\omega) = \frac{1 + N_1 i\omega + \ldots + N_n (i\omega)^n}{D_0 + D_1 i\omega + \ldots + D_d (i\omega)^d} \tag{5.1}$$

$$= N(i\omega)/D(i\omega) = N(s)/D(s)$$

where the coefficients N_ℓ, D_ℓ are *real constants*, and where n and d are the number of zeros and poles in the theoretical response. Briefly, we perform a least-squares fit of the estimated empirical function $\hat{T}_k = \hat{T}(i\omega_k)$ weighting each measurement inversely as the estimated variance. The coefficients N_ℓ, D_ℓ now give a compact and accurate description of the system's behavior, which can be computed at any desired frequency through (5.1). Furthermore, the roots of the polynomials $N(s)$ and $D(s)$ can be found by one of the standard algorithms (we used Bairstow's; see Acton, 1970), and these are good approximations to the zeros and poles of the actual system. They can be compared with the design values and in our experience the agreement has been gratifying.

It might be thought that a better way to find the poles and zeros would be to fit them directly to $\hat{T}_k$ -- without going through the intermediate step of determining the rational polynomial N/D. In our application (and

perhaps in many others) the determination of the real parameters N_ℓ , D_ℓ can be achieved through iterative solution of a *linear* least-squares system, which is highly stable.

Let us now consider the algorithm for finding N_ℓ and D_ℓ in more detail. The difference between the true response $T(i\omega_k)$ and the estimated one $\hat{T}_k$ is assumed to be normally and independently distributed in the real and imaginary parts with the same standard deviation σ_k . The value of σ_k is approximated from Equation (4.12) by

$$\sigma_k = r_{95}/1.96 \quad . \tag{5.2}$$

The estimates at each frequency are independent so that the sum of squared misfits will be distributed as χ^2 ; therefore we choose the values of N_ℓ , D_ℓ that minimize

$$\chi^2 = \sum_{k=1}^{m} \frac{1}{\sigma_k^2} \left| T(i\omega_k) - \hat{T}_k \right|^2 \quad . \tag{5.3}$$

Here the moduli correctly account for the complex nature of the variables and their statistics. This is not a linear system in the unknowns N_ℓ , D_ℓ , but if we express $T(i\omega)$ in terms of $N(i\omega)$ and $D(i\omega)$, the resultant equation can be solved by iteration:

$$\chi^2 = \sum_{k=1}^{m} \frac{\left| N(i\omega_k) - \hat{T}\, D(i\omega_k) \right|^2}{\sigma_k^2 \left| D(i\omega_k) \right|^2} \quad . \tag{5.4}$$

This equation can be viewed as a weighted *linear* least-squares system in which the weights are the denominator terms $\sigma_k^2 |D(i\omega_k)|^2$; of course D is also unknown, but we assume an initial guess value (say $D(i\omega) \equiv 1$) and then solve the linear system for N_ℓ , D_ℓ , thus obtaining $N(i\omega)$ and $D(i\omega)$. The corrected value for D is used again in the denominator and the process is repeated several times. This procedure has been found to converge very rapidly in practical cases. It can be shown, rather surprisingly, that the value of χ^2 to which this process converges is not the true minimum, but is nonetheless rather close. To complete the calculation, we perform a linear least-squares solution to the first-order perturbation of Equation (17) (Gauss-Newton method, p.267, Ortega and Reinboldt, 1970).

The overdetermined linear systems are solved by the Q-R method of successive Householder rotations (Lawson and Hanson, 1974). It is important to realize that the classical treatment via solution of the "normal equations" often fails completely because of finite computer precision, and this is a defect almost entirely avoided by the Q-R algorithm.

We may test the fitting procedure and the statistics of the errors in the value of χ^2 . The number of degrees of freedom is clearly given by $\nu' = 2m - n - d - 1$, since we fit $n + d + 1$ parameters, the coefficients in the polynomials. The expected value of χ^2 is ν' and if the actual value in a particular calibration falls too far from this we must suspect one of our assumptions. In our experience the behavior of χ^2 has been very satisfactory, thus confirming the validity of our analysis.

6. DATA LOGGER

The data system for this experiment was constructed around a DEC PDP 11/10 mini-computer. Figure 10 shows a block diagram of the system. The salient features of the various subsystems are listed in Table 2.

In its data logging mode, the system can record up to 16 channels at 100 times per second or less with an arbitrary mix of sample rates on different channels within the limits. The system is controlled by the real time clock which issues interrupts to the CPU every 10 ms. Various software counters in the CPU determine the command sequence issued to the multiplexer, A-D converter and the tape drive. The tape drive serves as the data storage medium while the floppy disk drive is used for program storage and initial CPU loading. It is not operated during the actual data logging activities.

The real time clock also generates the RB signal in synchronization with the interrupts it issues to the CPU. Thus, we are able to know the precise time at which transitions occur without a high data sampling rate on the RB signal. The data sampling rate is then set by consideration of the instrument output characteristics.

Table 2.

CPU	Digital Equipment Corporation PDP 11/10 with 32KB of core memory, 9 track tape interface, real time clock interface, data acquisition system interface.
Tape	Cipher Data Products Mark I tape system. 9 track, 800 BPI, 45 IPS 2400 ft. reel.
Clock	Our design real time clock with integral random binary generator. Outputs days, hours minutes, seconds crystal controlled with $\pm 10^{-7}$ accuracy. Separate interrupt output 10 ms or 50 ms and time interval output 1 sec to 15 min adjustable.
Data A-D	Phoenix Data Systems. 16 channels, 15 bit, 4 kHz throughput rate.
Disk Drive	Sykes model, dual floppy disk.
Operator's Console	DEC LA36 Decwriter (TTY equivalent), 300 Baud, 132 columns.

7. CALIBRATION PROCEDURE

The zero frequency system (loop) response we have shown to depend upon four instrument parameters. The nominal value of 516 $Vm^{-1} s^2$ was not verified experimentally but presumably could be via a tilting technique as is done with the IDA systems.

The cross-spectral calibration using a random binary signal gives the system's relative response as a function of frequency. Experimentally we calibrated the feedback loop in two steps, a high frequency run to determine the parameters with time constants shorter than 1 second and a low frequency run principally to determine the frequency response of the high pass data filter that is part of the down-hole package. The long period filter was calibrated separately.

The RB voltage is summed with the loop voltage through the calibration attenuator and the system's output voltage recorded along with the RB signal. It is the system's response to this first step which is subsequently used to estimate its impulse response.

The computational procedure that follows is illustrated in a block diagram in Figure 11.

Step 1: When the calibrating voltage is applied to the system at time zero an initial step occurs. The next step does not occur until 25 clock cycles of the RB generator. The system output for this period is considered to be its approximate step function response.

Step 2: The step function response is first-differenced to approximate the impulse response. This first-differenced step is then input into two separate procedures: Step 3 and Step 5.

Step 3. The differenced step is convolved with the RB signal to form e'_{out} (Figure 7), the approximate system output, which can be seen to be very close to e_{out}, the actual output.

Step 4. The cross-spectrum between e_{out} and e'_{out} is formed, which repates the actual output to the approximate output. Figure 12 illustrates how these two series are related as a function of frequency.

Step 5. The Fourier transform of the differenced step is corrected for the effect of differencing (versus true differentiation) and multiplied by the complex transfer function produced in Step 4 to yield the overall system transfer function. The associated errors are those of Step 4.

Step 6: The ratio of two polynomials of specified degree are least-squares fit to the system's transfer function. The degree of these polynomials is dictated by the parametric model. For the SRO systems the numerator has degree 1, corresponding to one zero and the denominator has degree 4, corresponding to 4 poles. The locations of the poles and zeros in the complex plane are:

Zero: $s = 0$;

Poles: $s = -.117$; -112 ; $-4.08 \pm i\ 3.67$.

The parametric model of the SRO system yielded

$$T_{pD}(s) = \left[\frac{2.59 \times 10^9}{s^2 + 8.50\ s + 32.6}\right] \cdot \left\{\frac{s(s + 50)}{(s + 100)\ (s + .118)\ (s + 41.4)}\right\}$$

for the "data output", that is the signal that is input to the LP and SP filters.

The zeros of this expression and the poles at $s = -100$ are determined by 1 percent circuit components. The pole at $s = -0.118$ is nearly independent of loop gain, varying from 0.120 to 0.117 for all reasonable values of that parameter. Therefore, in our high noise environment, our calibrating strategy was to assume the nominal positions for these poles and the two zeros. We evaluate

$$\frac{i\omega(i\omega + 50)}{(i\omega + .118)\ (i\omega + 100)}$$

at each Fourier harmonic ω_k and divide this out of the measured response. We then fit a 3 pole, no zero polynomial to the result. Recombining this result with the expression above we find the best fitting polynomial for the data output is

$$T_D(s) = \left[\frac{2.59 \times 10^9}{s^2 + 8.52\ s + 31.7}\right]\left\{\frac{s(s + 50)}{(s + 41.0)\ (s + .118)\ (s + 100)}\right\} \text{ V m}^{-1}\ \text{s}^2 \qquad (7.1)$$

and we may then deduce the mass position output polynomial by dividing this by T_5 (Equation (2.9)) to give

$$T_M(s) = \left[\frac{2.59 \times 10^4}{s^2 + 8.52\ s + 31.7}\right]\left\{\frac{(s + 50)\ (s + .125)}{(s + 41.0)\ (s + .118)}\right\} \text{ V m}^{-1}\ \text{s}^2\ . \qquad (7.2)$$

The quantity in the brackets is the dominant two pole approximation to the transfer function. It describes the response of a pendulum with a free period of .90 seconds damped .76 of critical. This is only an approximation, however, as the quantity in the braces contributes significantly to the response above 1 Hz.

It must be emphasized that in our calibration procedure we determined only the complex conjugate pole pair that constitutes the dominant two pole approximation and the pole at $s = -41.0$. The numerator constants in Equations (7.1) and (7.2) were estimated as described in Section 2.

The output voltage e_D is passed through two shaping filters before being recorded as the long period (LP) channel and the short period (SP) channel. In addition the LP channel passes through an anti-aliasing filter. The LP filter is an 8 pole, 4 zero network and the anti-aliasing filter is a 4 pole network (McGowan and Lacoss, 1978). Thus the overall LP transfer function may be written as

$$T_{LP}(s) = K_{LP} \sum_{k=0}^{6} a_k s^k \Big/ \sum_{k=0}^{17} b_k s^k \qquad (7.3)$$

where

$a_0 = 0$

$a_1 = 0$

$a_2 = 0$

$a_3 = 54.8$

$a_4 = 1.096$

$a_5 = 50.0$

$a_6 = 1.00$

$b_0 = 1.7042 \times 10^{-3}$

$b_1 = 3.0062 \times 10^{-1}$

$b_2 = 1.5458 \times 10^{1}$

$b_3 = 3.2677 \times 10^{2}$

$b_4 = 3.8120 \times 10^{3}$

$b_5 = 2.8133 \times 10^{4}$

$b_6 = 1.4031 \times 10^{5}$

$b_7 = 4.9221 \times 10^{5}$

$b_8 = 1.2388 \times 10^{6}$

$b_9 = 2.2481 \times 10^{6}$

$b_{10} = 2.9322 \times 10^{6}$

$b_{11} = 2.6564 \times 10^{6}$

$b_{12} = 1.5301 \times 10^{6}$

$b_{13} = 4.7162 \times 10^{5}$

$b_{14} = 7.7037 \times 10^{4}$

$b_{15} = 6.3416 \times 10^{3}$

$b_{16} = 1.5617 \times 10^{2}$

$b_{17} = 1.00$

The field calibration procedure (Jon Peterson, personal communication) is to set all stations to have an amplitude response of 5×10^3 counts per micron of ground displacement at a 25 second period. Thus in Equation (7.3) we set $s_0 = \frac{i2\pi}{25}$ and solve

$$|s_0^2 T_{LP}(s_0)| = 5 \times 10^9 \text{ counts m}^{-1} \tag{7.4}$$

to get

$$K_{LP} = 6.516 \times 10^{12} \text{ counts m}^{-1} \text{ s}^2 \quad .$$

The overall SP transfer function may be written as

$$T_{SP}(s) = K_{SP} \sum_{k=0}^{4} a_k s^k \Big/ \sum_{k=0}^{8} b_k s^k \tag{7.5}$$

where

$a_0 = 0$ $\qquad$ $b_2 = 1.5518 \times 10^9$

$a_1 = 0$ $\qquad$ $b_3 = 1.5598 \times 10^9$

$a_2 = 0$ $\qquad$ $b_4 = 8.3095 \times 10^7$

$a_3 = 50.0$ $\qquad$ $b_5 = 2.4229 \times 10^6$

$a_4 = 1.0$ $\qquad$ $b_6 = 3.8548 \times 10^4$

$b_7 = 3.1216 \times 10^2$

$b_0 = 1.7696 \times 10^{11}$ $\qquad$ $b_8 = 1.00$

$b_1 = 7.6799 \times 10^{10}$

For this channel, the outputs are normalized during field calibration to produce 2×10^6 counts per micron of ground displacement at a one second period. Thus in Equation (7.5) we set $s_0 = i2\pi$ and solve

$$|s_0^2 T_{SP}(s_0)| = 2 \times 10^{12} \text{ counts m}^{-1} \tag{7.6}$$

to get

$$K_{SP} = 2.090 \times 10^5 \text{ counts } m^{-1} s^2 \quad .$$

The stations at Taipai, Guam and South Karori have a 10^3 lower gain due to excessive local noise, so for these stations

$$K_{SP} = 2.090 \times 10^2 \text{ counts } m^{-1} s^2 \quad .$$

APPENDIX A

Digital Convolution of Random Binary Sequences and Calculation of T_0

A crucial step in the practical implementation of the cross spectrum calibration method is the digital filtering of the RB sequence to produce the signal e'_{out} . We want to make e'_{out} very much like the actual recorded output, e_{out} , so that the transfer function estimate is unbiased. Because of the broad band nature of the RB signal, it is not obvious that the digital convolution is permissable because of the problem of aliasing. We establish here the sampling requirements on the RB signal, and the method of approximating digitally the impulse response of the seismograph system so that the digital convolution yields exactly the sampled values of the output of the continuous system. It is also shown how to calculate T_0 , the initial estimate of the system transfer function by digital Fourier transforms.

If $e_c(t)$ is the random binary sequence, and $h(t)$ is the seismograph impulse response then the seismograph output at discrete times $n\Delta t$ is

$$e_{out}(n\Delta t) = \int_{-\infty}^{\infty} h(\tau)\, e_c(n\Delta t - \tau)\, d\tau \quad . \tag{A1}$$

For a suitable digital sequence $g(n\Delta t)$, the filtered version of the sampled RB sequence is

$$e'_{out}(n\Delta t) = \sum_{k=-\infty}^{\infty} g(k\Delta t)\, e_c(n\Delta t - k\Delta t) \quad . \tag{A2}$$

and we now give the conditions on g and e_c so that $e'_{out} = e_{out}$.

Consider first the seismograph response to the unit step function

$$s(t) = \int_{-\infty}^{\infty} h(\tau)\, U(t-\tau)\, d\tau \quad . \tag{A3}$$

A noisy record of $s(t)$ is provided by the first long interval of the RB sequence (see Figure 7, e_{out} for $0 \le t \le 200s$).

Let $g(n\Delta t)$ be the first backward difference of the sampled record of $s(t)$

$$g(n\Delta t) = \int_{-\infty}^{\infty} h(\tau) \left\{U(n\Delta t-\tau) - U(n\Delta t-\Delta t-\tau)\right\} d\tau \quad . \tag{A4}$$

Using Equation (A4) in (A2) and exchanging the order of summation and integration

$$e'_{out}(n) = \int_{-\infty}^{\infty} h(\tau) \sum_{k=-\infty}^{\infty} \left(U(k-\tau) - U(k-1-\tau)\right) e_c\,(n-k)\, d\tau \tag{A5}$$

where we have set $\Delta t = 1$. For Equation (A5) to equal (A1) we must show

$$\sum_{k=-\infty}^{\infty} \left(U(k-\tau) - U(k-1-\tau)\right) e_c\,(n-k) = e_c\,(n-\tau) \quad . \tag{A6}$$

Viewed as a function of continuous variable τ ,

$$U(k-\tau) - U(k-1-\tau) = \begin{cases} 0 & \tau < k-1 \\ 1 & k-1 \le \tau \le k \\ 0 & \tau > k \end{cases} \quad . \tag{A7}$$

But for $k - 1 \le \tau \le k$,

$$e_c\,(n-\tau) = e_c\,(n-k) \tag{A8}$$

provided that a) the RB clock period is an integral multiple of the sample interval Δt , and b) the RB clock is synchronized to the sample clock. Under these conditions Equation (A6) holds establishing the equality between Equations (A1) and (A2). Note that if the RB sequence were passed through an analog filter before sampling, Equation (A8) would not be true, and it is

only the binary nature of the RB sequence which makes the procedure work. With suitable relationships between the RB clock and the sample clock, higher order differences could be used for $g(n)$ but we have found the simple first order difference satisfactory.

The differenced step function response is a good approximation to the system impulse response, but the digital Fourier transform of $g(n)$ must be slightly modified to obtain T_0, the first estimate of the transfer function. Since

$$g(n) = s(n) - s(n-1) \tag{A9}$$

application of the shift theorem (Bracewell, 1965) yields

$$S(f) = \frac{G(f)}{1 - e^{-i2\pi f}} \tag{A10}$$

but T_0 is $i2\pi f$ times the transform of the system step response. Thus, for discrete frequencies $f = n/N$

$$T_0 = \frac{i2\pi n}{N} \frac{G}{1 - e^{-i2\pi n/N}} \quad . \tag{A11}$$

REFERENCES

Acton, F. S. (1970). *Numerical Methods That Work*, Harper and Row, New York.

Agnew, D. C. and J. Berger (1978). Vertical seismic noise at very low frequencies, *J. Geophys. Res.*, in press.

Berger, J., McCowan, D. W., Farrell, W. E. and R. T. Lacoss (1978) Comments on 'Transfer functions for the Seismic Research Observatory seismograph system' by D. W. McCowan and R. T. Lacoss, *Bull. Seism. Soc. Am.*, in press.

Bendat, J. S. and A. G. Piersol (1971). *Random Data: Analysis and Measurement Procedures*, Wiley, New York.

Haubrich, R. (1965). Earth noise 5 to 500 millicycles per second; Part I, Spectral stationarity, normality, and nonlinearity, *J. Geophys. Res.*, 70, 1415-1427.

Jenkins, G. M. and D. G. Watts (1968). *Spectral Analysis and its Applications*, Holden Day, San Francisco.

Lancaster, D. (1975). *TTL Cookbook*. Howard W. Sams & Co., Indianapolis.

MacWilliams, F. J. and N. J. Sloan (1976). Pseudo-random sequences and arrays, *Proc. IEEE*, 64, 1715-1729.

McCowan, D. W. and R. T. Lacoss (1978). Transfer functions for the Seismic Research Observatory seismograph system, *Bull. Seism. Soc. Am.*, 68, 501-512.

Moore, R. D. and W. E. Farrell (1970). Linearization and calibration of electro-statically fedback gravity meters, *J. Geophys. Res.*, 75, 928-932.

Munk W. H. and D. E. Cartwright (1966). Tidal spectroscopy and prediction, *Phil. Trans. Roy. Soc. Lond. A* **259**, 533-581.

Ortega, J. M. and W. C. Rheinboldt (1970). *Iterative Solution of Nonlinear Equations in Several Variables*, Academic Press, New York.

Teledyne Geotech (1975). *Operation and Maintenance Manual, Borehole Seismometer System Model 36000, Part I.*

FIGURE CAPTIONS

Figure 1. Block diagram of the SRO system. Accelerations a_g and a_f are summed by the inertial mass. The mass motion is detected and amplified to yield two outputs, e_{out} and e_D. Voltage e_{out} is filtered and summed with calibration voltage e_c to produce a feedback acceleration on the mass.

Figure 2. The top panel shows details of the system circuit enclosed in dashed lines in Figure 1. The lower panel shows details of the feedback portion of the loop.

Figure 3. SRO signal flow graph. This figure shows how Equations 2.1 through 2.8 are connected in the closed loop model. Unlabeled branches have a transfer function of unity.

Figure 4. Root locus plot of SRO system. This figure shows the second quadrant of the complex s-plane ($Re(s) < 0$, $Im(s) > 0$) . The open loop ($G = 0$) poles (x) occur at $s = -p_i$ and the zero (0) at $s = -z_i$ where p_i , z_i are listed in Table 1. As G increases, the poles move along the indicated curves. At an operating gain of $G = 352$, the dominant closed loop pole in this quadrant occurs at the position marked Δ .

Figure 5. Sensitivity of the dominant second quadrant SRO system pole to variations in ac gain, G_2 , compensator pole p_3 and zero z_3 . The portion of the root locus enclosed in the box in Figure 4 is expanded in this figure to show the effects of parameter variations from 5 percent below their nominal values (the labeled end of the curves) to 5 percent above their nominal values. Other loop parameters have a much smaller influence on the dominant pole positions.

Figure 6. SRO system Bode plots. These plots show the transfer function modulus (upper panel) of the system model outputs.

Figure 7. Voltage waveforms. e_c is an example of the random binary calibrating signal. An initial downward half step occurs at time zero followed by a long quiescent period before the next full step occurs. e_{out} is the system output voltage and the response to the initial half step is used as an approximation to the system step response. e'_{out} is the predicted system output. The wave forms illustrated were obtained from an IDA system.

Figure 8. The expected errors on system gain and phase as a function of the cross-spectral coherence $\hat{\gamma}^2_{12}$ and the number of degrees of freedom ν or the number of groups into which the time series are divided.

Figure 9. The expected phase and gain errors at a 95% confidence level, as a function of frequency with (lower trace) and without (upper trace) frequency dependent alignment. The large increase in the errors near 100 mHz corresponds to the first "hole" in the RB calibrating signal spectrum.

Figure 10. Block diagram of the data logging system.

Figure 11. Block diagram of the calibration computation. Up to the "cross-spectrum" box all computations are done in the time domain.

Figure 12. The results of the cross-spectrum of e_{out} and e'_{out}. The two traces show the 95% confidence limits on phase (upper panel) and gain (lower panel). The deviations of the quantities from 0° and 1.0 indicate the errors in the initial prediction of the system step response. As in Figures 3 and 6 the large fluctuations in these quantitites near 100 mHz are due to the decrease in input energy at the first "hole" of e_c. Note that f_n represents the operational Nyquist frequency for 20 second samples.

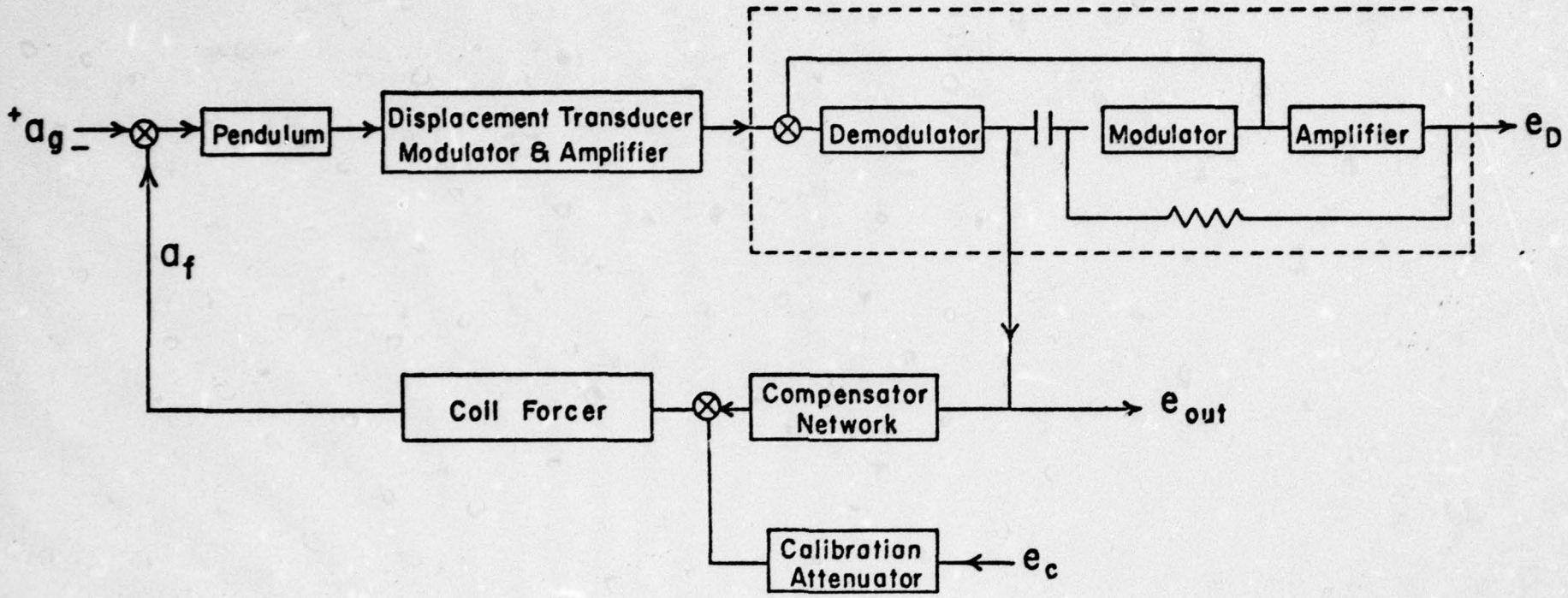
+a_g −
Pendulum
Displacement Transducer
Modulator & Amplifier
Demodulator
Modulator
Amplifier
e_D
a_f
Coil Forcer
Compensator
Network
e_out
Calibration
Attenuator
e_c

Figure 1.

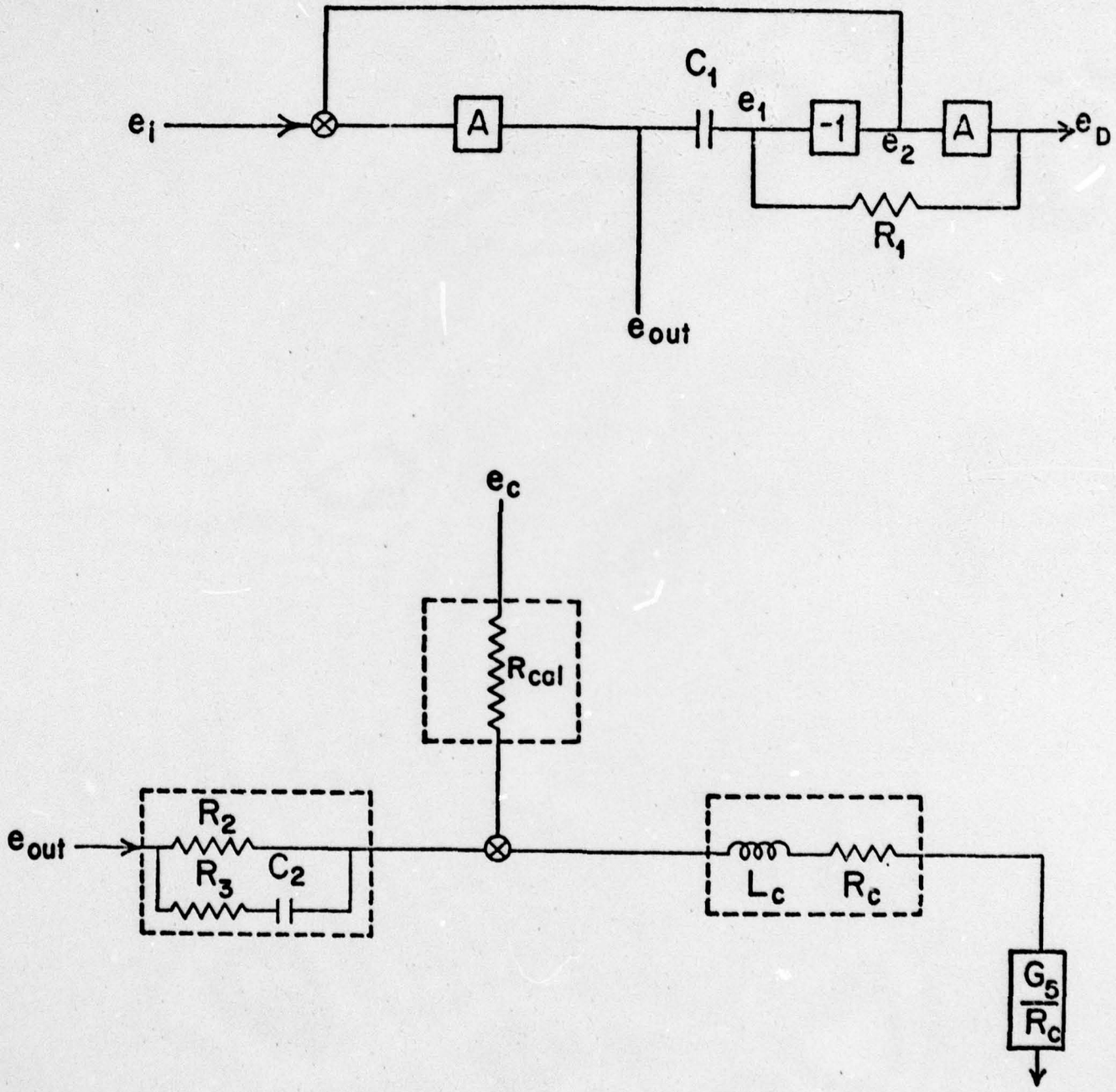

Figure 2.

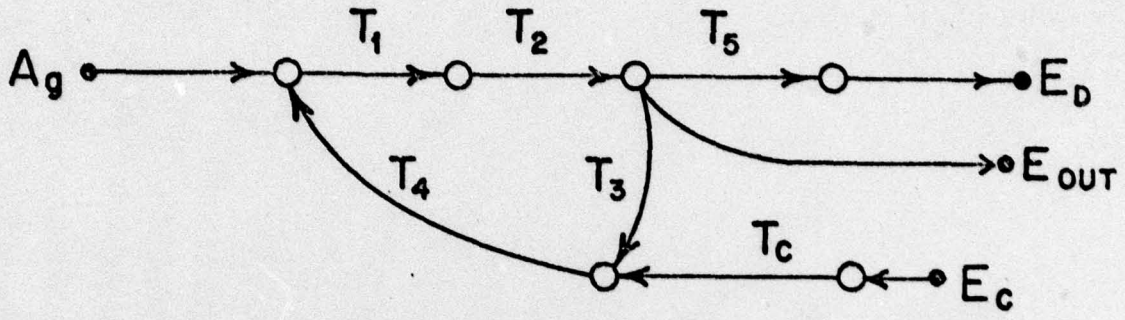

Figure 3.

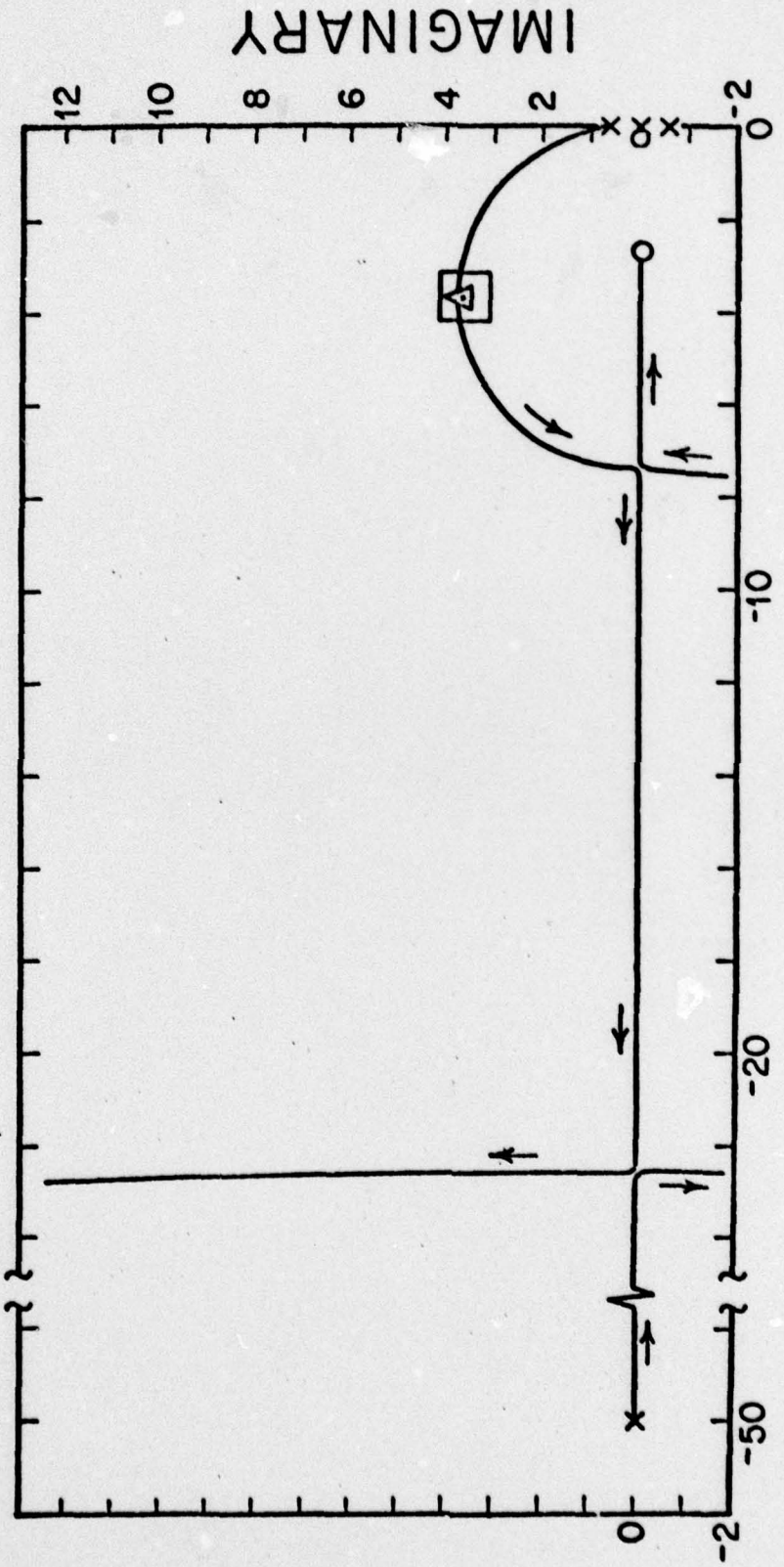

Figure 4.

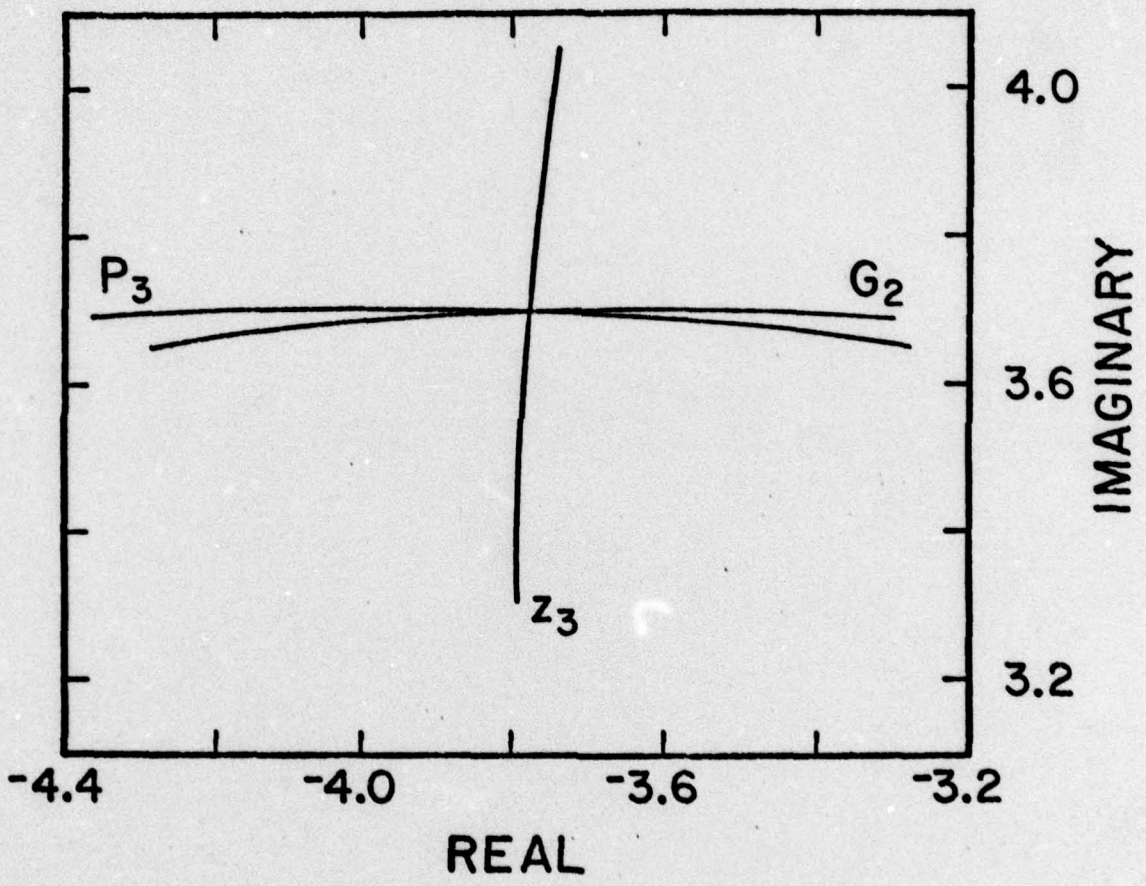

Figure 5.

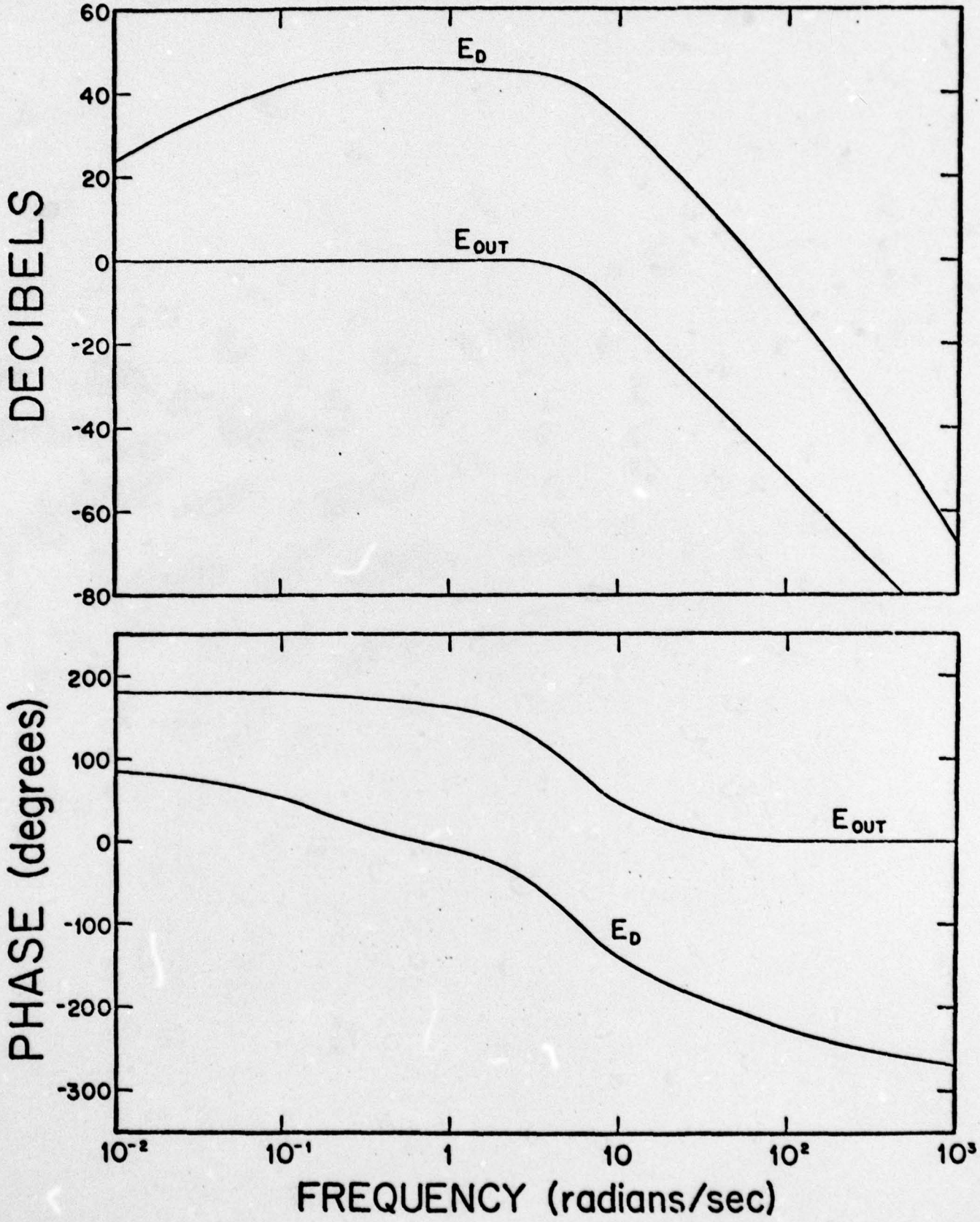
60
40
20
0
-20
-40
-60
-80
DECIBELS
E_D
E_{OUT}
200
100
0
-100
-200
-300
PHASE (degrees)
E_{OUT}
E_D
10^{-2}
10^{-1}
1
10
10^2
10^3
FREQUENCY (radians/sec)

Figure 6.

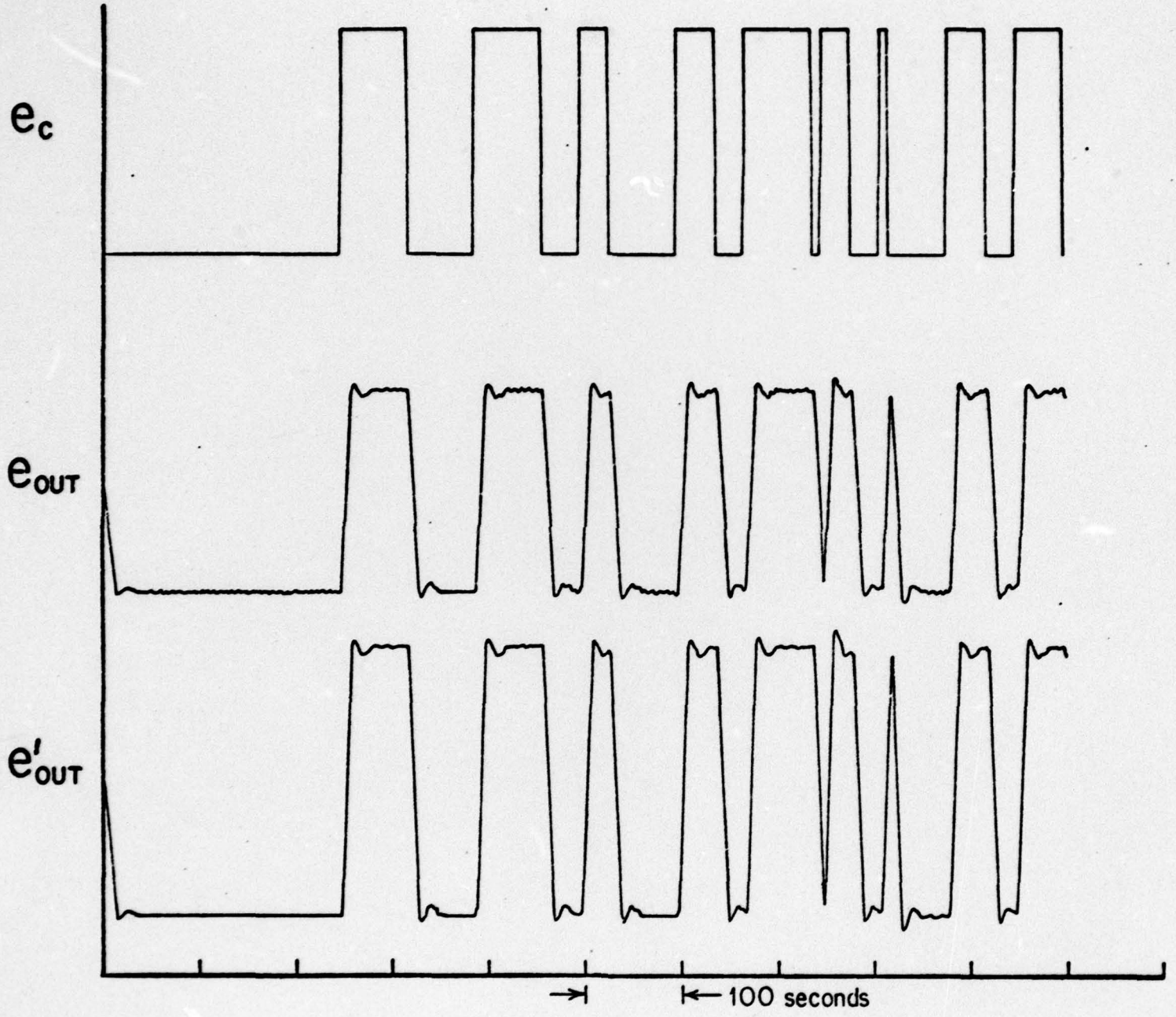

Figure 7.

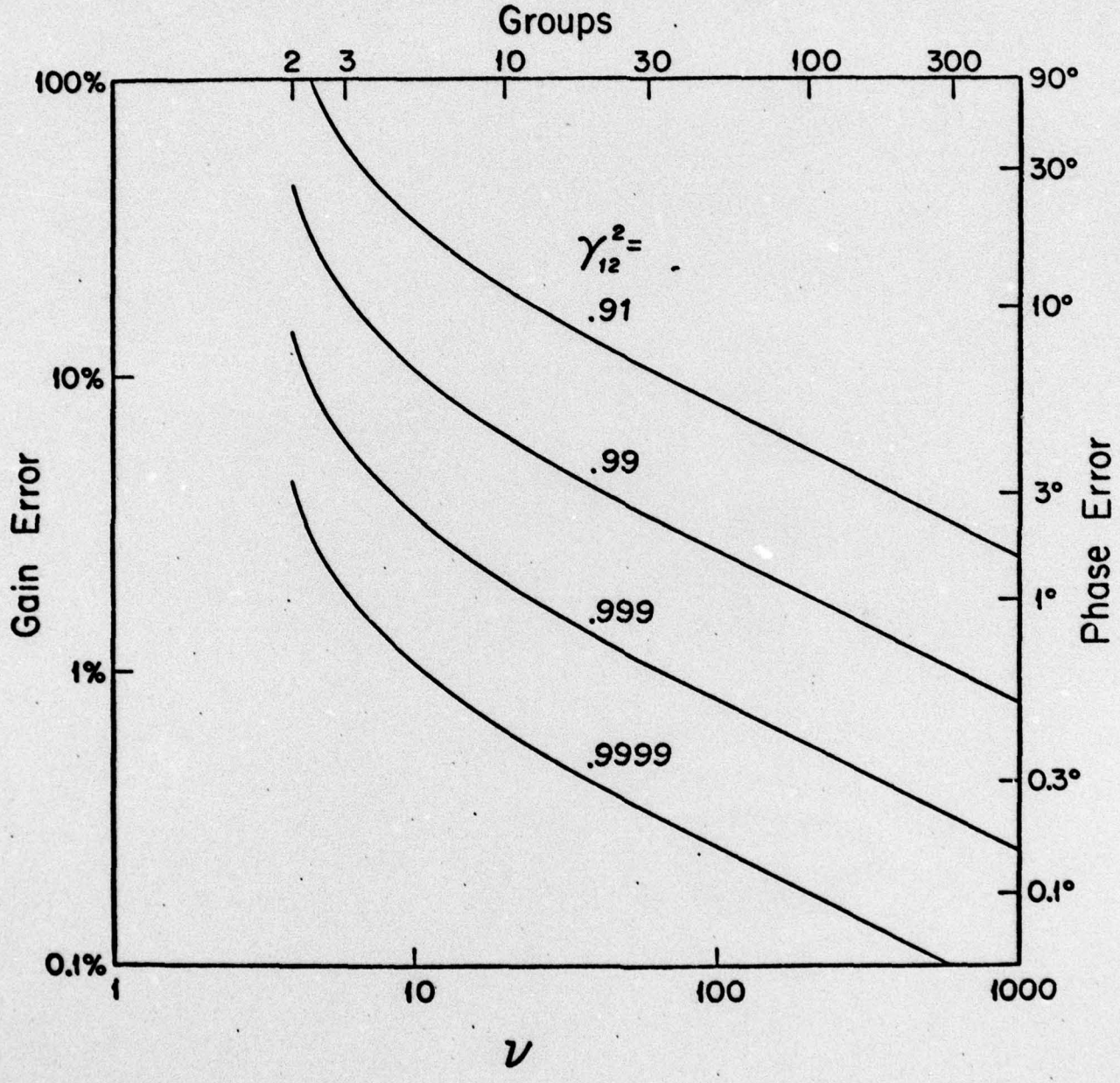
Groups
2
3
10
30
100
300
100%
10%
1%
0.1%
90°
30°
10°
3°
1°
0.3°
0.1°
Gain Error
Phase Error
γ_{12}^2=
.91
.99
.999
.9999
1
10
100
1000
ν

Figure 8.

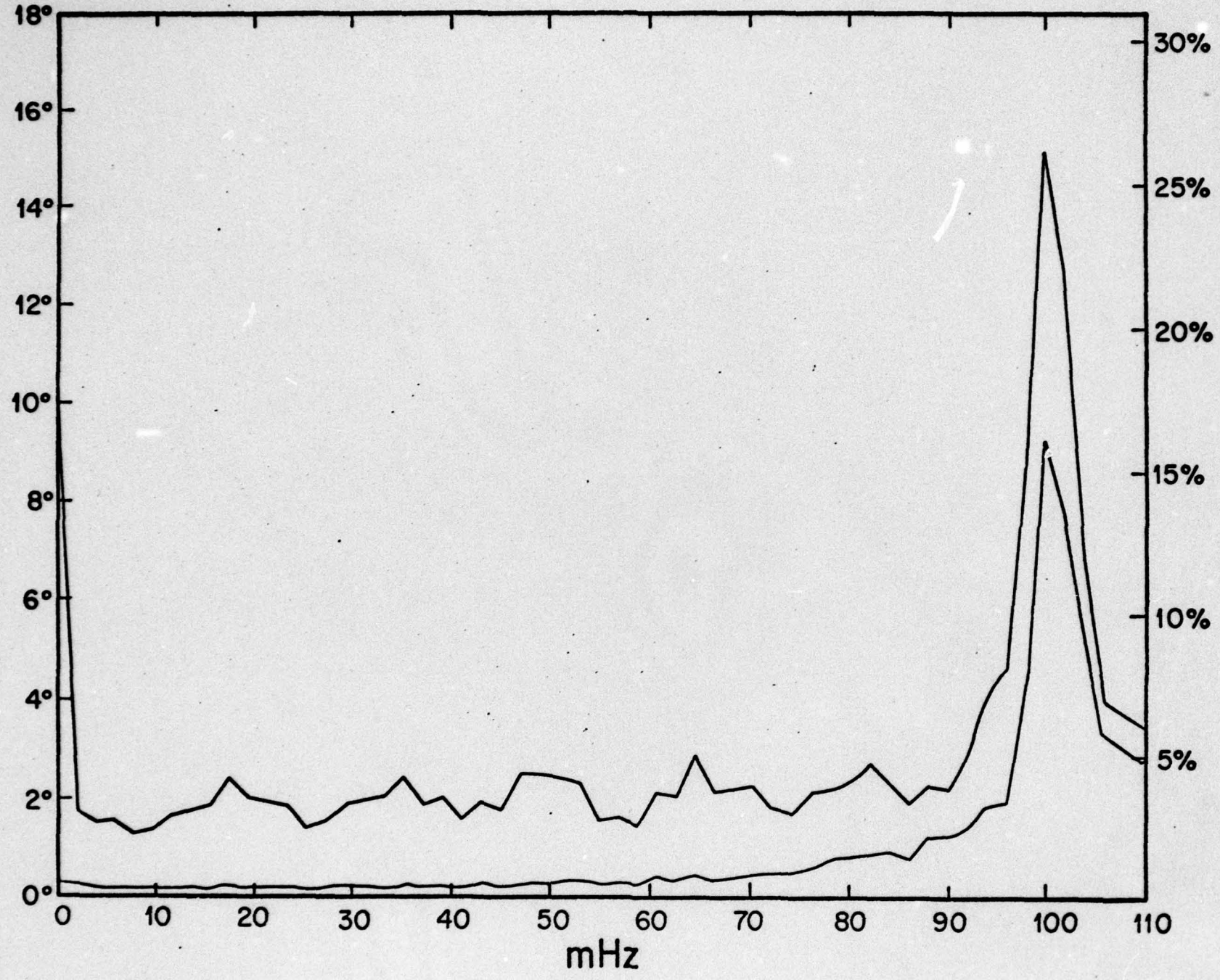
18°
16°
14°
12°
10°
8°
6°
4°
2°
0°
30%
25%
20%
15%
10%
5%
0
10
20
30
40
50
60
70
80
90
100
110
mHz

Figure 9.

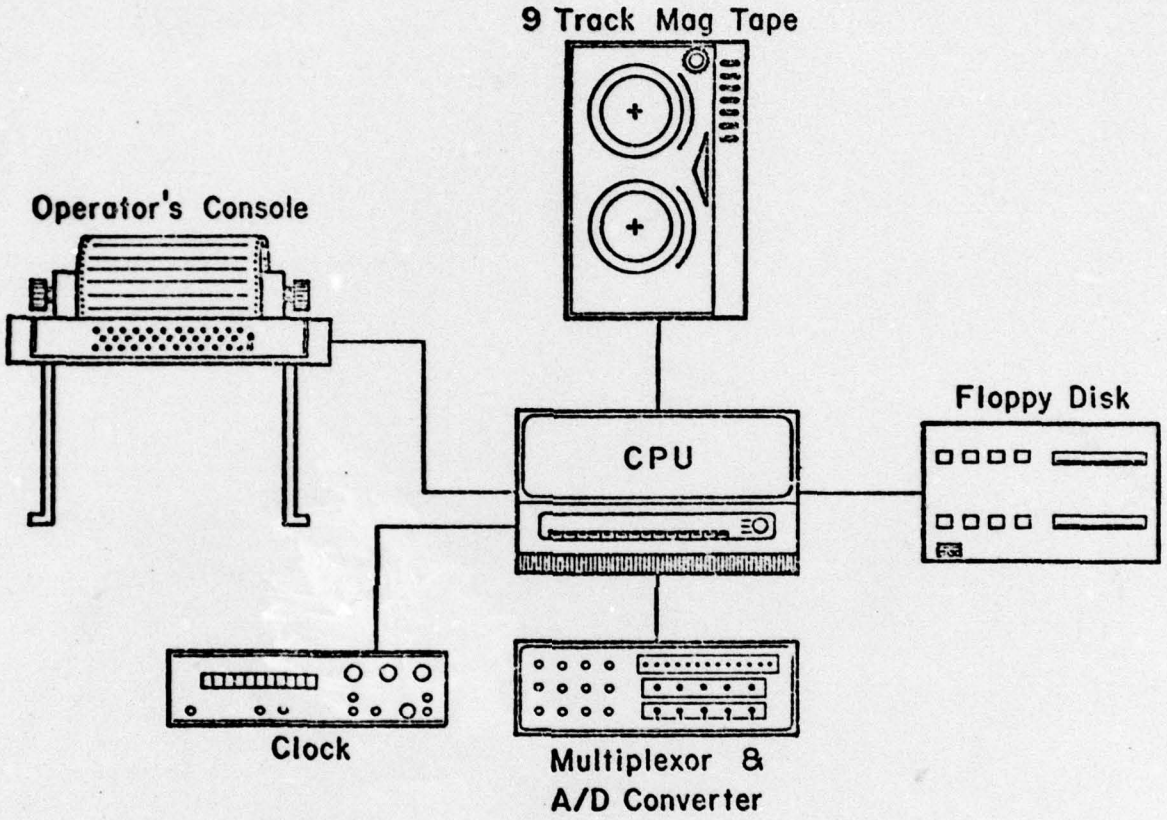

DATA LOGGING SYSTEM

Figure 10.

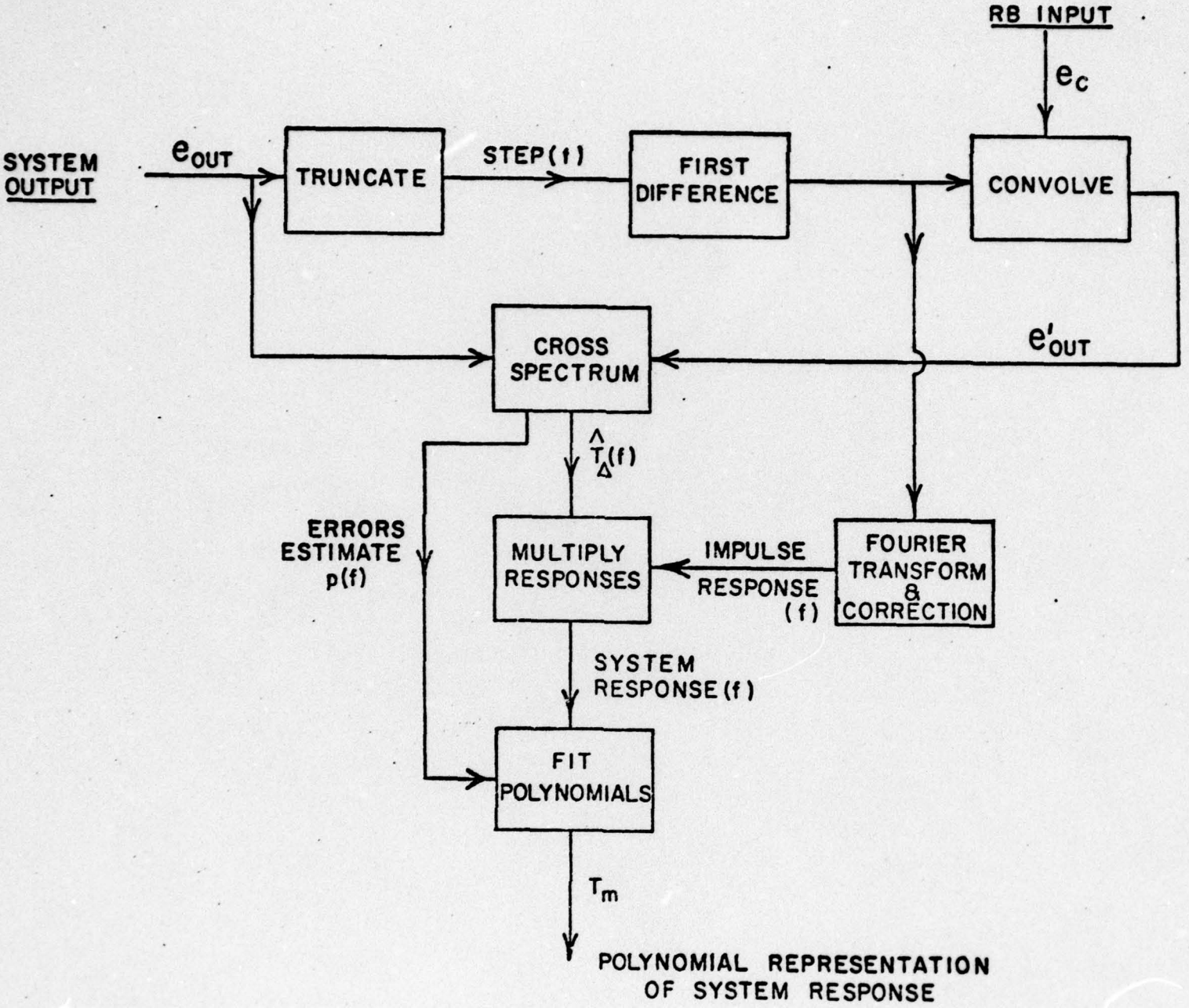
RB INPUT
e_c
SYSTEM OUTPUT
e_{OUT}
TRUNCATE
STEP(f)
FIRST DIFFERENCE
CONVOLVE
e'_{OUT}
CROSS SPECTRUM
$\hat{T}_\Delta(f)$
ERRORS ESTIMATE p(f)
MULTIPLY RESPONSES
IMPULSE RESPONSE (f)
FOURIER TRANSFORM & CORRECTION
SYSTEM RESPONSE(f)
FIT POLYNOMIALS
T_m
POLYNOMIAL REPRESENTATION OF SYSTEM RESPONSE

Figure 11.

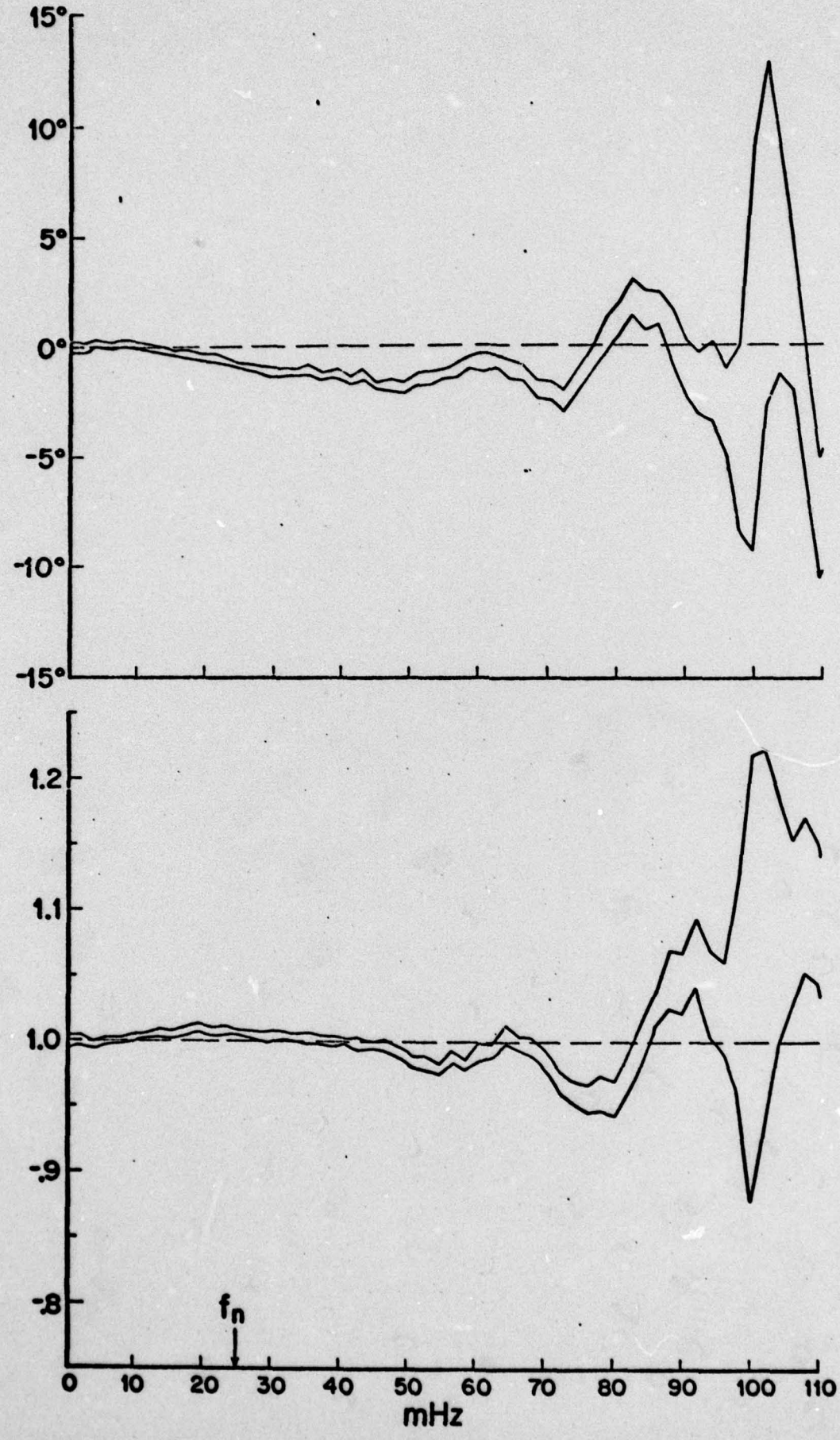

Figure 12.

ROUTING AND TRANSMITTAL SLIP		ACTION
1 TO (Name, office symbol or location) DDC/TCA/Mrs. Crumbacker	INITIALS	CIRCULATE
	DATE	COORDINATION
2	INITIALS	FILE
	DATE	INFORMATION
3	INITIALS	NOTE AND RETURN
	DATE	PER CONVERSATION
4	INITIALS	SEE ME
	DATE	SIGNATURE

REMARKS

Attached is a revised AFOSR-TR-78-1013. Please destroy the old one you have which had ADA054788 and use this new one.

Sig by ——

AD A058661

Do NOT use this form as a RECORD of approvals, concurrences, disapprovals, clearances, and similar actions.

FROM (Name, office symbol or location)	DATE
AFOSR/XOPD Karlene Blose Bolling AFB, DC 20332	11 Sep 78
	PHONE 767-4912

OPTIONAL FORM 41
AUGUST 1967
GSA FPMR (41CFR) 100-11.206

GPO 043—16—81418-1 418-016 5041-101